Advancement in Science and Technology Research
Vol. 2(1), pp. 1-7, January 2015
Full Length Research Paper

Fabrication and numerical simulation of a quadrupoles sintered Alnico 5 magnet

Solaf Abi-Eisha and Mustafa Eleoui*

Higher Institute for Applied Sciences and Technology, P. O. Box 31983, Damascus, Syria.

Accepted 19 January, 2015

ABSTRACT

In this study, an Alnico 5 quadrupoles magnet was manufactured by powder metallurgy followed by heat treatment in an external applied magnetic field. A physical model for the distribution of magnetization was proposed inside the magnet. Then the finite elements method, using the FlexPDE software package, was applied to deduce the magnetic field profile created by the magnet. The magnetic flux and magnetic induction near one pole of the magnet was measured, and a good agreement was found with the simulated results.

Keywords: Alnico, magnetic simulation, magnetization model, powder metallurgy.

*Corresponding author. E-mail: mustafa.eleoui@hiast.edu.sy.

INTRODUCTION

Recent research are being carried out nowadays to find relevant magnetic materials which can replace rare earth magnets in technological applications, such as motors, generators and microphones, in order to be able to operate at high temperatures (>180°) and reduce their costs. Because of their specific properties, Alnico alloys are subjects of new researches as a possible candidate (Zhou et al., 2014).

Alnico alloys are one of the major classes of permanent magnet materials. These alloys vary widely in composition and in preparation to give a broad spectrum of properties, costs and workability. Generally, Alnicos are superior to other permanent magnet materials in resisting temperature effects on magnetic performance. Alnico magnets containing more than 24% Co are the only group of magnetically hard materials that can be treated thermally in an external applied magnetic field (Davis, 1990; Wohlfarth and Buschow, 2001). This process results in formation of anisotropic structures and magnetic hardening effect (Stanek et al., 2010).

Alnico 5 is one of the most important commercial alloys of this family. It contains 50% Fe, 24% Co, 14.5% Ni, 8.5% Al and 3% Cu. An energy product of $(BH)_{max}$ = 42 kJ/m^3 is indicative of the excellent magnetic properties of these alloys when thermally treated in a magnetic field (Davis, 1990).

Alnico alloys are usually fabricated by sand or shell-mold casting; a few are fabricated by powder metallurgy techniques (Rosenberg, 1968). Sintered Alnico is produced by blending powders, pressing and sintering just below the melting temperature in an oxygen-free atmosphere. The sintered alloys have mechanical properties superior to those of cast Alnicos, but the magnetic properties generally are slightly lower (Davis, 1990). Pre-alloyed powder can also be used to fabricate Alnico magnet by powder metallurgy techniques. In this case, the powder is produced by melting of the magnetic alloys, casting, crushing and controlled milling to single domain particles (Landolt and Börnstein, 2003).

MATERIALS AND METHODS

Sintered Alnico 5 magnets were manufactured, starting from pre-alloyed powders. Parts made from pre-alloyed powders have a homogeneous microstructure and uniform apparent hardness (Asm International Handbook Committee, 1998). Firstly, Alnico 5 bars (previously manufactured by casting) were crushed and milled using tumbling ball mill for 18 h (mill engine power is 5 kW and its rotational speed is 1440 rpm). Powder was then sifted and only powder having size between 20 µm and 50 µm

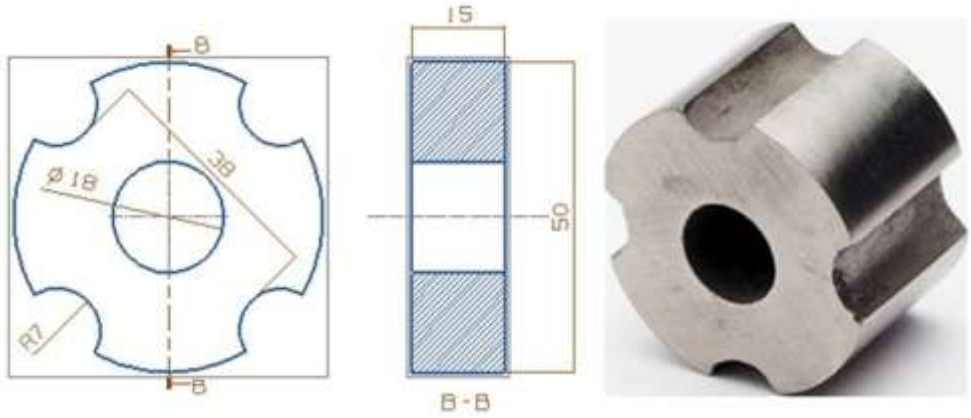

Figure 1. The quadrupoles manufactured magnet.

were used in the experiments. These powders have been investigated by XRD using a Philips (PW3710) diffractometer using a Cu x-ray tube (Kα1 and Kα2 $\lambda_1 = 1.54060$ Å, $\lambda_2 = 1.54439$Å) in the range $20° \leq 2\theta \leq 120°$ with a step of $0.01°$/s.

This ground powder was granulated by bonding material (a solution obtained by mixing rubber with benzol for more than 40 days) and then press-formed by using a vertical pressure of 50 tons into a form of quadrupoles magnet as in Figure 1, and the formed magnets were sintered for 2 h at the temperature of 1280°C.

These sintered magnets were subjected to a thermo-magnetic treatment in two steps as follows: annealing at a temperature of 920°C for 0.5 h followed by cooling down to 600°C with a rate of 25°C/min, this cooling was done in presence of an external magnetizing force of 160 kA/m. Then an aging treatment was carried out at a temperature of 650°C for 10 h, then at a temperature of 560°C for 20 h.

While cooling in the first step, a spinodal decomposition of the alloy, into a magnetic Fe–Co-rich (α1) phase and an Al-Ni-rich (α2) phase, occurs. The applied magnetic field enhance anisotropic growth of the α1 phase, which gives rise and enforces shape anisotropy in the magnet (Zhou et al., 2014).

In order to ensure homogeneity of density and absence of defects (cracks, inclusions), the final magnet was imaged by X-ray radiography (Asm International Handbook Committee, 1998).

Magnetic flux and induction near one of the poles of the magnet was measured by a flux meter and a tesla meter respectively.

In order to characterize the magnetic field created by the magnet, it is necessary to know the magnetization configuration inside it. This configuration could be hardly revealed theoretically, one can think to find a configuration that minimize the magnetic energy of the magnet by solving micro-magnetism equations, but this theory can be applied practically in submicron thin film elements and in nano-structures only (Hubert and Schäfer, 2009). In larger structures, as the current quadrupoles magnet, one can propose a configuration that agrees with the physical phenomena predicted in the magnet, such as magnetic moments should align with the external magnetic field, where a field is applied, are grouped in magnetic domains of parallel directions to minimize exchange energy and parallel to the surface of the sample to minimize demagnetizing effects by avoiding the creation of magnetic poles.

Here is proposed an approximate configuration of magnetization inside the magnetized quadrupoles magnet, taking into account the previous constraints. In this model, the distribution of magnetization is divided into four similar regions, with opposite directions as resumed in Figure 2, in every region the magnetic moments are supposed tangent to a circle concentric with the side circle between two adjacent poles. For example, in the region of center (x_0,0) in Figure 2 the magnetization is given by:

$$\boldsymbol{M} = \begin{cases} M\dfrac{y}{\sqrt{(x-x_0)^2+y^2}} \\ M\dfrac{-(x-x_0)}{\sqrt{(x-x_0)^2+y^2}} \end{cases} \text{for } (y < x \text{ and } y > -x)$$

Similar formula are applicable in the other three regions. The value of *M* depends on many factors as the density and composition of the material and the magnetic field applied during heat treatment. Here *M* is imposed after comparison of the simulated flux value with the measured flux near one of the poles as we will show subsequently.

Using this model, we deduced magnetic field and induction maps by finite element method employing the FlexPDE software package (P.S. Committee, 2011). We determine the magnetic vector potential $\boldsymbol{A}$, which is continuous in space. We have $\boldsymbol{B} = \boldsymbol{\nabla} \times \boldsymbol{A}$, and $\boldsymbol{H} = \boldsymbol{B}/\mu_0 - \boldsymbol{M}$**.** One can demonstrate that the potential vector $\boldsymbol{A}$ verifies the following equation (P.S. Committee, 2011):

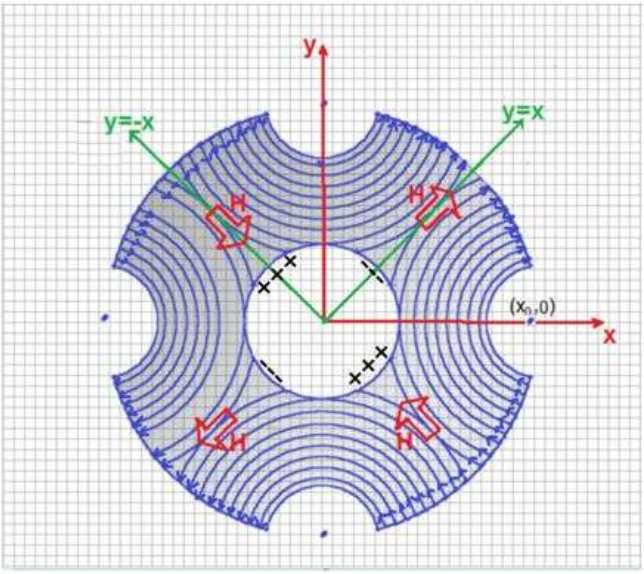

Figure 2. Configuration of Magnetization inside the magnet. The big arrows indicate directions of an external magnetic field applied during heat treatment.

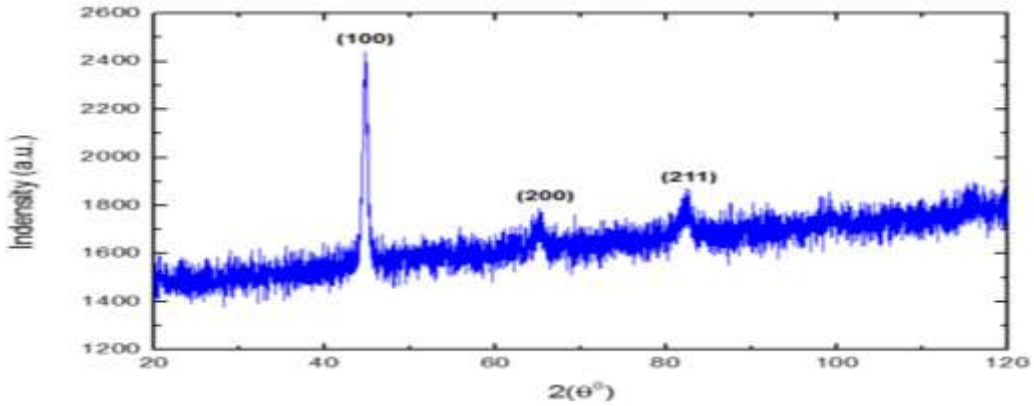

Figure 3. XRD profile of the Alnico 5 powder.

$$\boldsymbol{\nabla}.[\boldsymbol{\nabla A}/\mu_0 + [\boldsymbol{N}]] + \boldsymbol{J} = \boldsymbol{0} \quad (1)$$

Where $\boldsymbol{J}$ is the free current density ($\boldsymbol{J} = \boldsymbol{0}$ here) and $[\boldsymbol{N}]$ is the following tensor:

$$[\boldsymbol{N}] = \begin{pmatrix} 0 & 0 & -M_y \\ 0 & 0 & M_x \\ M_y & -M_x & 0 \end{pmatrix}$$

Equation 1 could be written in Cartesian coordinates as:

$$\boldsymbol{\nabla}.[\boldsymbol{\nabla} A_x/\mu_0 + \boldsymbol{N_x}] = \boldsymbol{0} \quad (2)$$

$$\boldsymbol{\nabla}.[\boldsymbol{\nabla} A_y/\mu_0 + \boldsymbol{N_y}] = \boldsymbol{0} \quad (3)$$

$$\boldsymbol{\nabla}.[\boldsymbol{\nabla} A_z/\mu_0 + \boldsymbol{N_z}] = \boldsymbol{0} \quad (4)$$

Where $\boldsymbol{N_x}, \boldsymbol{N_y}, \boldsymbol{N_z}$ are the rows of $[\boldsymbol{N}]$. The resolution of theses equations is done in large domain compared with the dimensions of the magnet, and a null potential vector is imposed on the limits of that domain assuming that at infinity the potential vector tends to zero (Jianming, 2002).

RESULTS AND DISCUSSION

Structural characterization

Figure 3 shows the obtained XRD profile for Alnico 5 powder. Obviously, the sample contains the α phase only and contains no γ phase that deteriorates the magnetic properties (Zhang et al., 2006). From this profile, we can

Figure 4. X-ray radiography of a final quadruoles magnet.

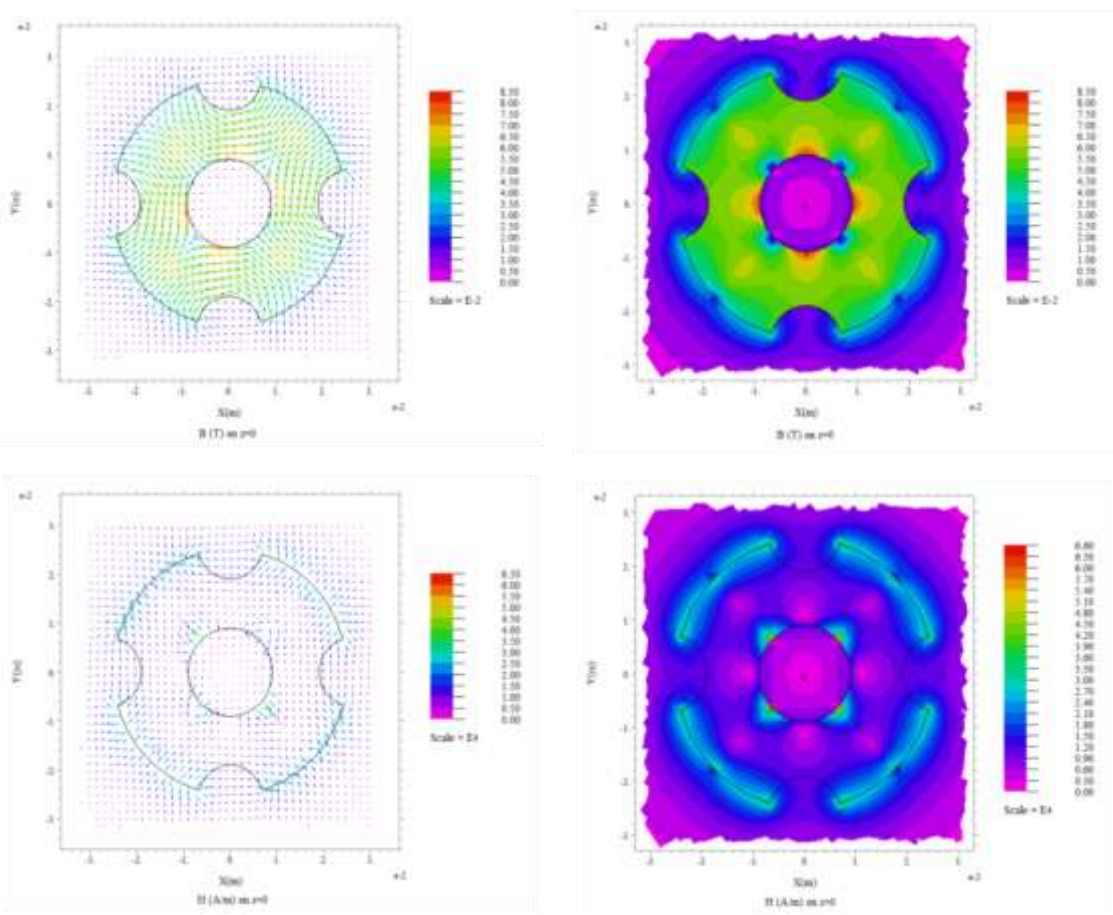

Figure 5. Magnetic induction *B* and magnetic field *H* created in a cross-section in the middle of the manufactured magnet.

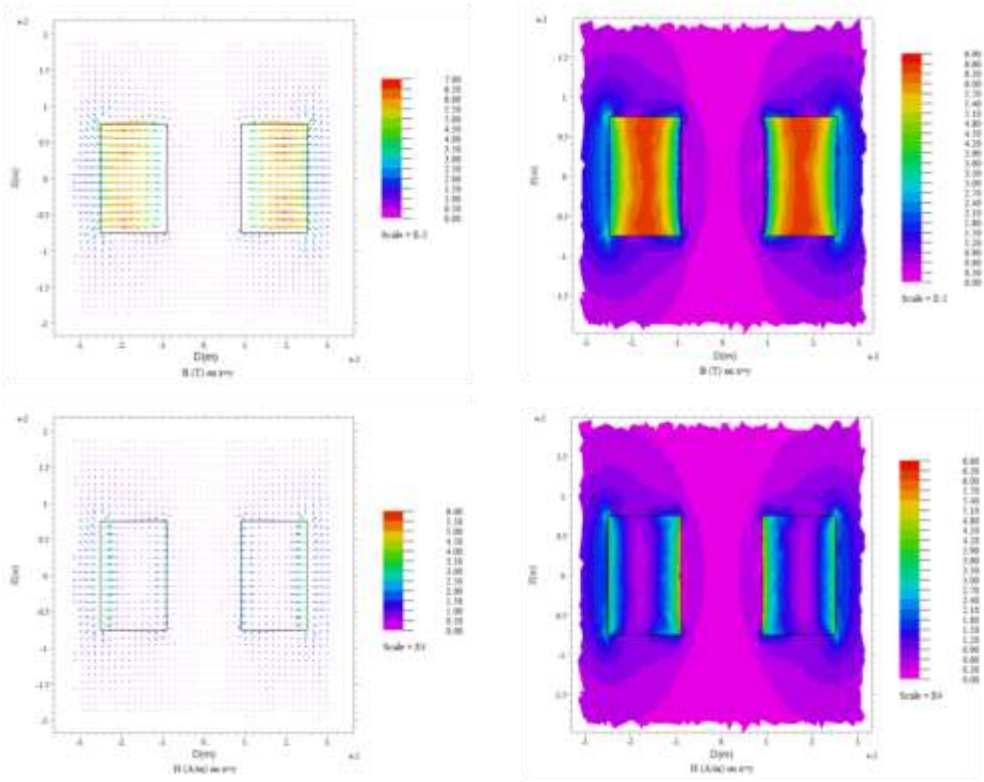

Figure 6. Magnetic induction *B* and magnetic field *H* created in the plan y = x.

get an indication that used powders have single domain particles. Indeed using Scherrer formula (Birkholz et al., 2006) one can deduce the grains mean size D:

$$D = \frac{k\lambda}{\beta cos\theta}$$

Where $k \cong 0.9$ assuming spherical crystallites, and β is the FWHM peak width corrected by the broadening due to the instrument. We found $D \cong 16$ nm. So, theses crystallites are smaller than the critical diameter for single domain particle in Alnico 5 (32 nm) (Wohlfarth, 1982), which means that particles have single magnetic domains. This small particle size is favorite to get maximum coercivity and remanence values (Aldabbagh et al., 2011).

Figure 4 shows an x-ray radiography image for one sample of the manufactured magnets. It is clear that this sample has no defects (cracks, inclusions), and has no density variations.

Magnetic characterization

Magnetic flux through a ring (100 turns, section area 6.2 cm^2) put face to one of the poles, was measured and a value of $\Phi = 0.9$ mWeb was obtained. We simulated the ring (Figure 7c) and the value of the magnetization *M* was adjusted to obtain the measured value of magnetic flux. A magnetization *M* = 54.35 kA/m was obtained and was used in the simulation. The magnetic induction near one pole has been measured too, and it is presented in Figure 7.

Magnetic simulation

Figures 5 and 6 show the simulation results of the magnetic induction *B* and the magnetic field *H* in two planes respectively. One can see that the magnetic field inside the magnet is opposing to the magnetization, as predicted by theory, and its value is between 0 and 66 kA/m. The lines of the magnetic induction *B* are directed from the N poles to the S poles, and its intensity is between 0 and 85 mT. Both *B* and *H* intensities decrease as the distance from the center increases. This is in good agreement with the measured results shown together with the simulated ones in Figure 7.

Figure 8 show more details for the magnetic induction intensity B on three different lines. In Figure 8a, the magnetic induction is zero in the central region of the magnet (the hole). This is a result of the proposed model of *M* which imposes similar "magnetic charges" on opposed faces (Figure 2). The magnetic induction has a maximum value approximately at the interior tangent

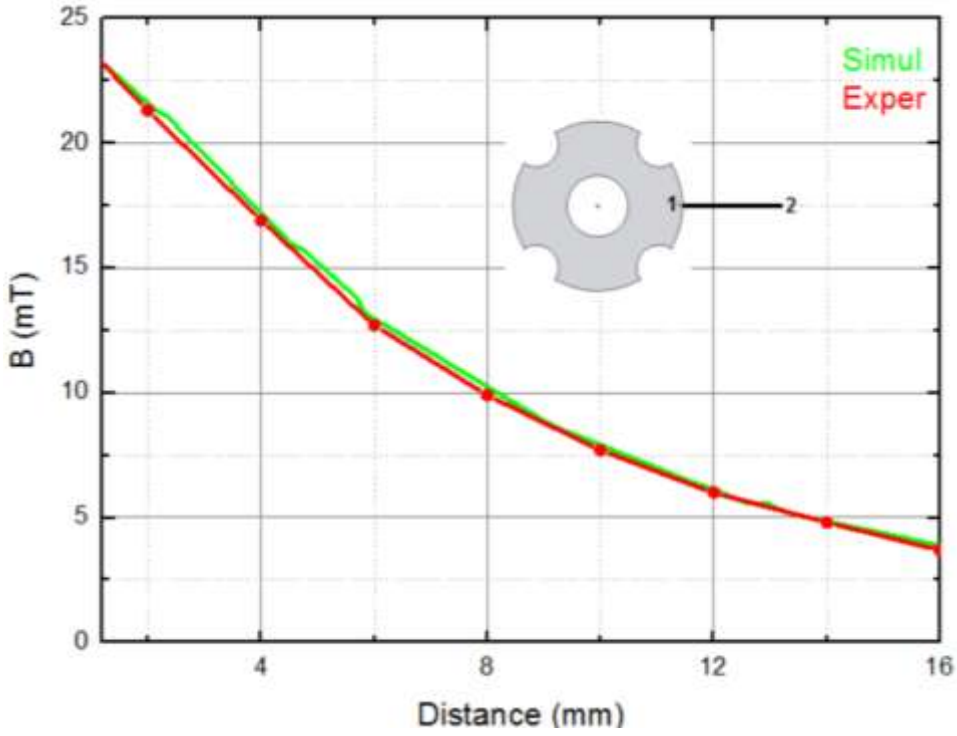

Figure 7. Simulated and measured magnetic induction intensity on the line 1-2 near one pole of the magnet, as function of the distance from point 1.

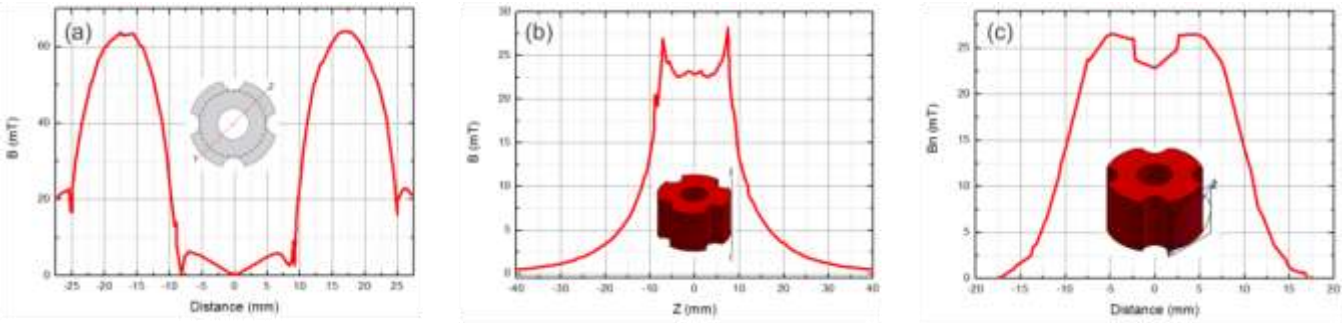

Figure 8. Magnetic induction intensity.

circle shown in Figure 8a. In Figure 8b, one can see that the magnetic induction is approximately uniform, near the poles, along length of the magnet, and its value decreases gradually when moving away from two sides of the magnet. This decrease is a general trend as seen in Figure 6. Finally, Figure 8c shows the ring used to simulate the magnetic flux near one pole. One can estimate a mean value for B of about 15 mT and compute an average value for the magnetic flux through the unique ring to find 93×10^{-5} Web, which gives 0.93 mWeb in 100 similar adjacent rings. This flux is computed in the simulation by numerical integration of *B* over the ring without using this averaged value.

The studied magnet is usually used inside a motor, so it will be useful to visualize the magnetic induction as the magnet rotates around the z-axis. Because the magnet is fixed in this simulation, one can get the magnetic induction variation on any fixed point, P, in the space (Figure 9a), by finding its values on a circle passing by P, and centered on the z-axis. Figure 9 shows the magnetic induction intensity *B* and its components on such a circle.

CONCLUSION

An Alnico 5 quadrupoles magnet was manufactured by powder metallurgy. XRD measurements demonstrated a single phase in the prepared powders (the α phase) with

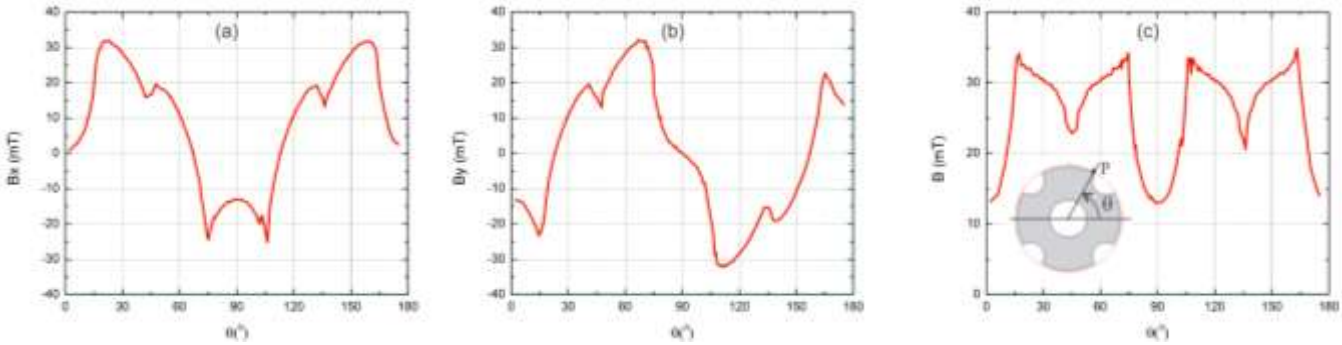

Figure 9. Magnetic induction on a circle of radius 26 mm: (a) *Bx*, (b) *By* (c) *B*.

small crystallites (16 nm). The magnet was simulated by FEM using an approximate model for the configuration of magnetization inside it. The simulated results are in good agreement with the experiment. The proposed model of *M* and the effectuated simulation could be useful, as seen in this paper, to estimate the needed magnetization value inside the magnet, in order to get a desired magnetic flux. This will give indication about the best material to fabricate the magnet. This work could also be of great importance in simulations of motors used in technological applications.

ACKNOWLEDGEMENT

We would like to express thanks to the team of HIAST, for their collaboration and facilities provided during this work.

REFERENCES

Aldabbagh JB, Jassim I, Odeh I, **2011**. Effect of Annealing Temperature on Magnetic and Structural Properties of ALNICO-5 Alloy. International Proceedings of Chemical, Biological and Environmental Engineering (IPCBEE), 25:6-10.

Asm International Handbook Committee, **1998**. Powder Metal Technologies and Applications. Vol. 7: ASM International.

Birkholz M, Fewster PF, Genzel C, **2006**. Thin Film Analysis by X-Ray Scattering. Weinheim: Wiley-VCH.

Davis JR, **1990**. Properties and selection: nonferrous alloys and special-purpose materials. ASM International.

Hubert A, **Schäfer** R, **2009**. Magnetic Domains. Berlin Heidelberg New York: Springer-Verlag.

Jianming J, **2002**. The finite element method in electromagnetics. New York: John Wiley & Sons, Inc.

Landolt H, **Börnstein** R, **2003**. Metals and Magnets. Landolt-Börnstein: Numerical Data and Functional Relationships in Science and Technology - New Series, Part 2A1. Vol. 2. Springer-Verlag Berlin Heidelberg.

P. S. Committee, **2011**. FlexPDE 6. PDE Solutions Inc.

Rosenberg SJ, **1968**. Nickel and its alloys. National Bureau of Standards.

Stanek M, Wierzbicki L, Leonowicz M, **2010**. Investigations of thermo-magnetic treatment of AlNiCo 8 alloy. Arch Metallurgy Mater, 55:571-577.

Wohlfarth EP, **1982**. Handbook of Magnetic Materials. Vol. 3. North-Holland Publishing Company.

Wohlfarth EP, **Buschow** KHJ, **2001**. Ferromagnetic Materials: A Handbook on the Properties of Magnetically Ordered Substances. North-Holland Publishing Company.

Zhang B, Lu G, Feng Y, Xiong J, Lu H, **2006**, Electromagnetic and microwave absorption properties of Alnico powder composites. Journal of Magnetism and Magnetic Materials, 299:205–210.

Zhou L, Miller MK, Lu P, Ke L, Skomski R, Dillon H, Xing Q, Palasyuk A, McCartney MR, Smith DJ, Constantinides S, McCallum RW, Anderson IE, Antropov V, Kramer MJ, **2014**. Architecture and magnetism of alnico. Acta Materialia, 74:224-233.

Citation: Abi-Eisha S, Eleoui M, 2015. Fabrication and numerical simulation of a quadrupoles sintered Alnico 5 magnet. Adv Sci Tech Res, 2(1): 1-7.